J. Fluid Mech. (1972), *vol.* 55, *part* 1, *pp.* 163–175
Printed in Great Britain

Viscous interaction over concave and convex surfaces at hypersonic speeds

By S. MOHAMMADIAN

Aeronautics Department, Imperial College, London†

(Received 21 August 1971 and in revised form 20 March 1972)

The growth of hypersonic boundary layers over both concave and convex surfaces is described, the strong-viscous-interaction equation due to Cheng *et al.* (1961) for curved surfaces with sharp leading edges being solved asymptotically for small and large arguments. Both the asymptotic solution for large arguments and a numerical integration predict an oscillatory behaviour of the boundary-layer thickness on concave surfaces. A modification of Cheng's theory, as suggested by Sullivan (1968) and Stollery (1970), is also examined and compared with experimental data reported here. The experiments were conducted in air using a hypersonic gun tunnel under cold wall conditions at $M_\infty = 12{\cdot}25$. They included measurement of surface pressure, heat-transfer distributions and schlieren studies for concave and convex models.

1. Introduction

At high Mach numbers the effects of compression and energy dissipation produce considerable increases in temperature. This causes the boundary layer to become very thick, but rapid changes of boundary-layer growth can occur near sharp leading edges and in regions of strong pressure gradients. The interaction between boundary-layer growth and the external inviscid flow can significantly modify the distribution of surface pressure and the heat-transfer rate. Therefore it is necessary to predict such mutual interaction before the body shape can be correctly designed to give a required performance and to withstand severe pressure and heating loads. The aim of this work is to enhance such predictions by comparing theory and experiments for hypersonic laminar flow over two-dimensional curved surfaces with sharp leading edges.

2. Experimental work

Surface-pressure and heat-transfer measurements were made using the no. 1 hypersonic gun tunnel in the Aeronautics Department of Imperial College. Stollery (1966) and Needham (1963) describe this facility and its capabilities. The measurements were carried out at a Mach number of 12·25 with a stagnation condition of $p_0 = 1600$ psia, $T_0 = 1300$ °K and a Reynolds number $R = 0{\cdot}86 \times 10^5$.

† Present address: Mechanical Engineering Department, Arya-Mehr University, Teheran, Iran.

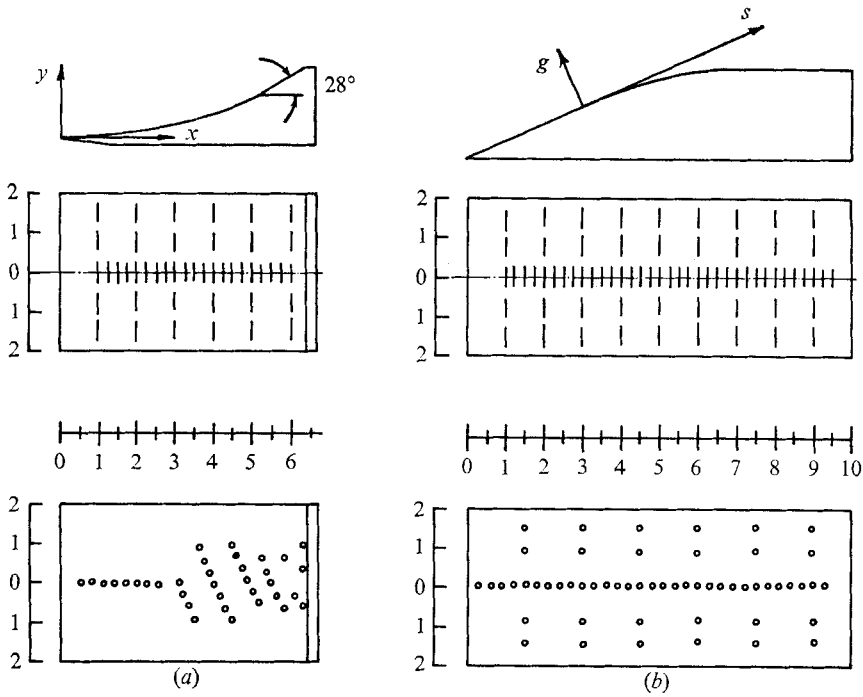

FIGURE 1. Layout of the models. (*a*) Concave heat-transfer and pressure models, $y = \frac{1}{150}x^3$, scale in inches. (*b*) Convex heat-transfer and pressure models; the fairing 3 in. downstream of the 18° wedge is $g = 0{\cdot}0026s^4 - 0{\cdot}0211s^3$ with the first and second derivatives equal to zero at the joining points with the two flat parts of the model.

The calibration of the Mach 12 contoured nozzle was carried out by Mohammadian (1968). Surface-pressure measurements were made using strain-gauge transducers, while thin-film platinum resistance thermometers were used to measure the surface temperature during the run. The gauges were coupled into a Wheatstone-bridge circuit and the out-of-balance voltage, due to the change in resistance of the gauges with temperature, was amplified and fed into an electronic analog circuit. The analog circuit solves the thermal-diffusion equation to give the heat-transfer rates as a function of time. Full details of the theory and development of the electronic apparatus have been reported by Holden (1964) and Hunter (1969). Models used for the present experimental study were cubic concave and convex, the co-ordinates and the layout of the models being given in figure 1. Figure 2 (plate 1) shows the pressure and heat-transfer models. The running time with steady flow was about 15 ms.

The flow over the models was attached and laminar, according to the schlieren photographs and heat-transfer traces. Typical schlieren pictures of the flow over concave and convex models at $M_\infty = 12{\cdot}25$ are shown in figures 3 and 4 (plate 2). The light line in the schlieren photograph appears because the schlieren system is sensitive to $\partial\rho/\partial y$ and, in hypersonic boundary layers, the maximum density gradient occurs towards the outer edge. The outer edge of this line in the schlieren picture is very close to the outer edge of the boundary layer and can be taken as a measure of the boundary-layer thickness. Boundary-layer profiles of Pitot

pressure, measured by Needham (1963) at a Mach number of $M = 9{\cdot}7$, confirm the above argument. Spanwise heat-transfer measurements showed that the flow was reasonably two-dimensional over both concave and convex surfaces.

3. Analysis

At hypersonic speeds, because of the thick boundary layer, the effective body shape can no longer be taken as the surface of the body and the surface of the body plus the displacement thickness of the boundary layer must be used. Therefore the viscous interaction effects must be considered to be as important as the first-order effects in any boundary-layer calculation involving a thick layer.

Three sets of equations are required to represent this type of flow: boundary-layer equations, inviscid-flow equations and a coupling equation. These equations can be summarized by the following three functional relations:

$$\delta^* = f_1(p_e), \tag{1}$$

$$p_e = f_2(y_e), \tag{2}$$

$$y_e = f_3(\delta^*), \tag{3}$$

where δ^* is the displacement thickness, $y_e\,(= y_e(x))$ is the effective body position for the inviscid flow and p_e is the pressure at that position. Hence a complete solution for the flow over a given shape $(y_w = y_w(x))$ is possible once methods of estimating the boundary-layer growth, external pressure distribution and effective-body streamline have been found.

By combining Lees' (1956) similarity solution for the boundary-layer growth with the Newton–Busemann inviscid equation (Cox & Crabtree 1965) and assuming that the effective body shape is the surface of the body plus the displacement thickness $(y_e = y_w + \delta^*)$, we obtain the following equation, which is known as Cheng's (1961) viscous-interaction equation:

$$(y_e - y_w)\,[(y_e y_e')^{\frac{1}{2}}]' = \left(\frac{\bar{\chi}_c^2 x}{4\gamma M_\infty^4}\right)^{\frac{1}{2}}, \tag{4}$$

where

$$\bar{\chi}_c = 0{\cdot}664(1 + 2{\cdot}6T_w/T_0)\,\bar{\chi}$$

and

$$\bar{\chi} = M_\infty^3 \sqrt{(C/R)}.$$

$\bar{\chi}$ is the viscous interaction parameter, T_w and T_0 are wall and total temperature respectively, C is the constant of proportionality in the linear viscosity–temperature relation and R is the Reynolds number based on distance x from the leading edge. The primes in (4) denote differentiation with respect to x.

For a family of shapes $y_w \sim x^n$ Stollery (1970) scales the above equation to give

$$(z - \xi^n)\,[(zz')^{\frac{1}{2}}]' = 1, \tag{5}$$

where

$$z_w = \xi^n, \quad z = y/\alpha l, \quad \xi = x/l$$

and

$$l = \bar{\chi}_c^2/4\gamma\alpha^4 M_\infty^4,$$

α being the angle of incidence. In terms of the new variables z and ξ the expressions for the pressure, the displacement thickness and the Stanton number St become

$$p/p_\infty/\gamma\alpha^2 M_\infty^2 = (zz')',$$
$$\delta^*/\alpha l = (z-\xi^n),$$
$$\frac{A\,St}{1{\cdot}328\gamma\alpha^3} = \frac{1}{z-\xi^n}.$$

Equation (5) is singular at the origin and admits the solution $z = \xi^n$ for $\xi \neq 0$. This is the behaviour to be expected when the displacement effect predominates (Lees 1953; Stewartson 1955). With an asymptotic solution for $\xi \to 0$ known, the solution to the (5) can be obtained by forward integration from the origin using Runge–Kutta or predictor–corrector methods.

The asymptotic solution to (5) for $\xi \to 0$ is

$$z = 2(\tfrac{4}{3})^{\frac{1}{4}}\xi^{\frac{3}{4}} + \frac{3}{8n^2+2n}\xi^n + \ldots. \tag{6}$$

The derivation of this equation can be found in the Ph.D. thesis of the author (1970). The first term in (6) is the flat-plate solution for zero incidence and is the predominant term for $\xi \to 0$. For $n > 1$ the second term in the solution can be neglected without introducing much error, first because, as $\xi \to 0$, ξ^n becomes much smaller than $\xi^{\frac{3}{4}}$ and second because the coefficient of ξ^n decreases with increasing n. For $n = 1$, i.e. a flat plate at an incidence, (6) reduces to

$$z = 2(\tfrac{4}{3})^{\frac{1}{4}}\xi^{\frac{3}{4}} + \tfrac{3}{10}\xi + \ldots. \tag{7}$$

For $\xi = 0{\cdot}001$ the second term in the above solution is 10 % of the first term and for $\xi = 0{\cdot}0001$ it is only 1·5 %. Therefore for a sufficiently small argument the flat-plate solution may be taken as the starting value with reasonable accuracy.

The author (1970) and Stollery (1970) have shown that the numerical solution of Cheng's equation over concave surfaces oscillates for large arguments. Similar oscillatory behaviour has been noted by Cheng & Kirsch (1969) in their study of intense explosions. This oscillatory behaviour may be examined by asymptotic solution of the equation for large arguments.

4. Asymptotic solution of Cheng's equation for large arguments

The equation to be solved asymptotically is the scaled version of Cheng's viscous-interaction equation; namely equation (5). We now put $\Delta^* = z - \xi^n$, where Δ^* is the scaled displacement thickness, and by rewriting (5) in terms of Δ^* obtain

$$\Delta^*\{[(\Delta^* + \xi^n)(\Delta^{*\prime} + n\xi^{n-1})]^{\frac{1}{2}}\}' = 1. \tag{8}$$

An asymptotic solution of Δ^* as $\xi \to \infty$ can be obtained if we assume that $\Delta^* \to 0$, which means that this analysis applies for concave surfaces only. We now rewrite (8) as

$$\Delta^*\left\{\left[n\xi^{2n-1}\left(\frac{\Delta^*\Delta^{*\prime}}{n\xi^{2n-1}} + \frac{\Delta^*}{\xi^n} + \frac{\Delta^{*\prime}}{n\xi^{n-1}} + 1\right)\right]^{\frac{1}{2}}\right\}' = 1,$$

which, for $\Delta^* \to 0$ as $\xi \to \infty$ gives

$$\Delta^*[(n\xi^{2n-1})^{\frac{1}{2}}]' = 1, \tag{9}$$

and on differentiation

$$\Delta^* = \frac{2}{n^{\frac{1}{2}}(2n-1)}\xi^{\frac{3}{2}-n}. \tag{10}$$

The above expression for Δ^* reveals an interesting phenomenon. Decaying solutions of the displacement thickness Δ^* exist only for $n > \frac{3}{2}$ as $\xi \to \infty$, i.e. there are some compression surfaces where the displacement thickness increases with increasing distance far from the leading edge. We shall discuss this characteristic in detail in the next section.

We now rewrite Δ^* as

$$\Delta^* = z - \xi^n - \frac{2}{n^{\frac{1}{2}}(2n-1)}\xi^{\frac{3}{2}-n}, \tag{11}$$

and substitute in (8) to obtain

$$\begin{aligned}\tfrac{1}{2}(\Delta^* + D\xi^{\frac{3}{2}-n})[(\Delta^* + \xi^n + D\xi^{\frac{3}{2}-n})(\Delta^{*\prime} + n\xi^{n-1} + E\xi^{\frac{1}{2}-n})]' \\ = [(\Delta^* + \xi^n + D^{\frac{3}{2}-n})(\Delta^{*\prime} + n\xi^{n-1} + E\xi^{\frac{1}{2}-n})]^{\frac{1}{2}},\end{aligned} \tag{12}$$

where $D = 2/n^{\frac{1}{2}}(2n-1), \quad E = (3-2n)/n^{\frac{1}{2}}(2n-1).$

After differentiation we approximate the resulting equation for $\Delta^* \to 0$ and $\xi \to \infty$ and obtain the following second-order ordinary differential equation with variable coefficients:

$$\xi^2\frac{\partial^2\Delta^*}{\partial\xi^2} + \frac{2n+1}{2}\xi\frac{\partial\Delta^*}{\partial\xi} + \frac{n^{\frac{1}{2}}(2n-1)^2}{2}\xi^{2n-\frac{3}{2}}\Delta^* = 0. \tag{13}$$

This equation is identical to the generalized Bessel equation

$$x^2y'' + x(a+2bx^r)y' + [c + dx^{2s} - b(1-a-r)x^r + b^2x^{2r}]y = 0, \tag{14}$$

with the oscillatory solution

$$y = x^{\frac{1}{2}(1-a)}e^{-bx^r/r}y_\rho(dx^s/s), \tag{15}$$

where $y_\rho = A_1J_\rho + A_2J_{-\rho}, \quad \rho = (1/s)\{\tfrac{1}{4}(1-a)^2 - c\}^{\frac{1}{2}}.$

On comparing (13) with (14) we find that

$$a = \tfrac{1}{2}(2n+1), \quad b = 0, \quad c = 0,$$

$$d = \tfrac{1}{2}n^{\frac{1}{2}}(2n-1)^2, \quad s = n - \tfrac{3}{4}, \quad \rho = (1-2n)/(4n-3).$$

Hence

$$\Delta^* = \xi^{\frac{1}{4}(1-2n)}[A_1J(X) + A_2J_{-\rho}(X)], \tag{16}$$

where

$$X = 2\frac{(2n)^{\frac{1}{2}}(2n-1)}{4n-3}\xi^{n-\frac{3}{4}},$$

and A_1 and A_2 are constants. Equation (16) clearly demonstrates the oscillatory behaviour of Δ^* for large arguments.

5. Discussion

The results of the numerical solution of Cheng's equation for some concave surfaces are plotted in figure 5. This figure demonstrates clearly the oscillatory behaviour of Cheng's equation, which was shown analytically in the previous

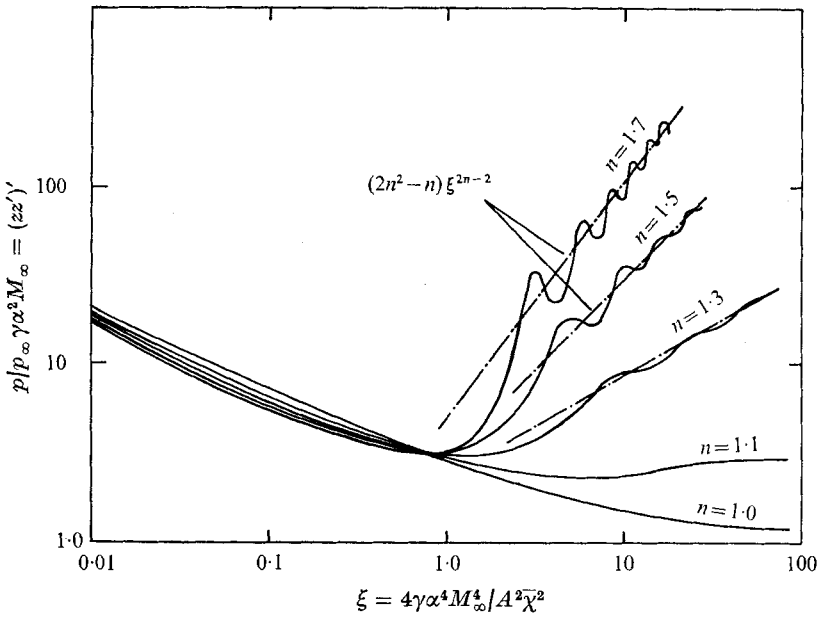

FIGURE 5. Theoretical prediction of pressure for a family of shapes $y_w \sim x^n$.

section. The stronger the concave nature of the surface the higher is the frequency of the oscillations but the oscillations damp out quickly in the downstream direction. As the flow moves along the surface the dominant influence changes from that of displacement to that of incidence. For small ξ, or $A^2\bar{\chi}^2 \gg \alpha^4 M_\infty^4$, the boundary layer being governed by the displacement effect, the pressure drops despite the concave nature of the surface. For large ξ ($\alpha^4 M^4 \gg A^2\bar{\chi}^2$), the dominant effect being incidence, the pressure should approach the inviscid value with the geometric surface of the body as the effective body shape. Therefore

$$p_e/p_\infty \gamma\alpha^2 M_\infty^2 = (z_w z_w')',$$

and with $z_w = \xi^n$ we obtain

$$p_e/p_\infty \gamma\alpha^2 M_\infty^2 = (2n^2-n)\,\xi^{2n-2}.$$

This equation is in fact the equation of lines about which the pressure curve oscillate and which appear as straight lines in figure 5. Similar results can be obtained for the boundary-layer growth and heat-transfer rate, since these are functions of the pressure ratio.

Cheng's equation does not give oscillating solutions for convex surfaces, as was demonstrated by Stollery (1970) and Mohammadian (1970). In the study of viscous interaction over a convex corner, Sullivan (1968) and Stollery (1970) modified Cheng's method by using the tangent-wedge approximation instead of the Newton–Busemann pressure law. Their results show that the modified Cheng method does not yield oscillating solutions when applied to concave and convex surfaces. This suggests that the cause of the oscillatory behaviour resulting from Cheng's method in its original form is the centrifugal correction in the Newton–Busemann pressure formula.

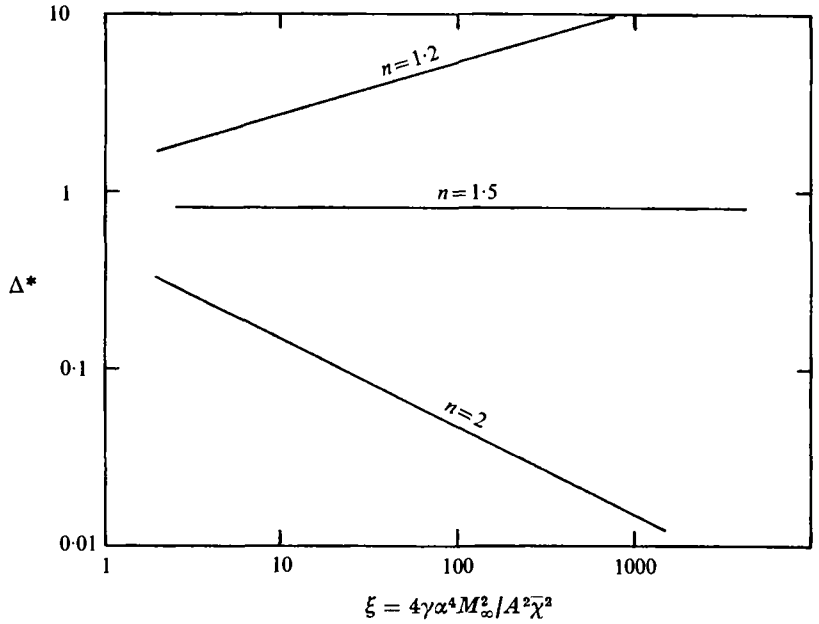

FIGURE 6. Theoretical prediction of displacement thickness over concave surfaces $z_w = \xi^n$.

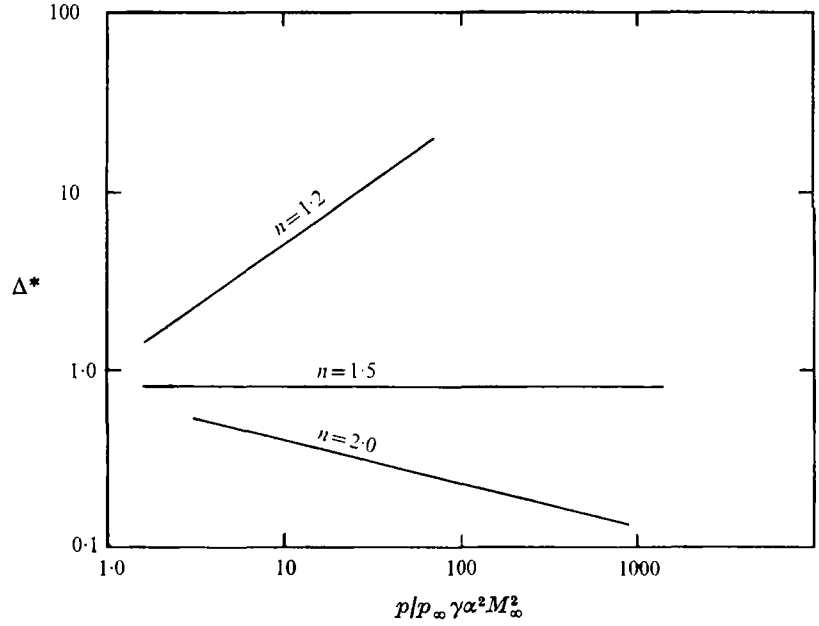

FIGURE 7. The distribution of the scaled displacement thickness as a function of pressure ratio for concave surfaces $z_w = \xi^n$ obtained by Cheng's method.

6. Super- and subcritical behaviour of the boundary layer

Perhaps the most striking feature of Cheng's method in its original form, as well as in the modified version, is the super- and subcritical behaviour of the boundary-layer growth over concave surfaces. (A boundary layer is said to be

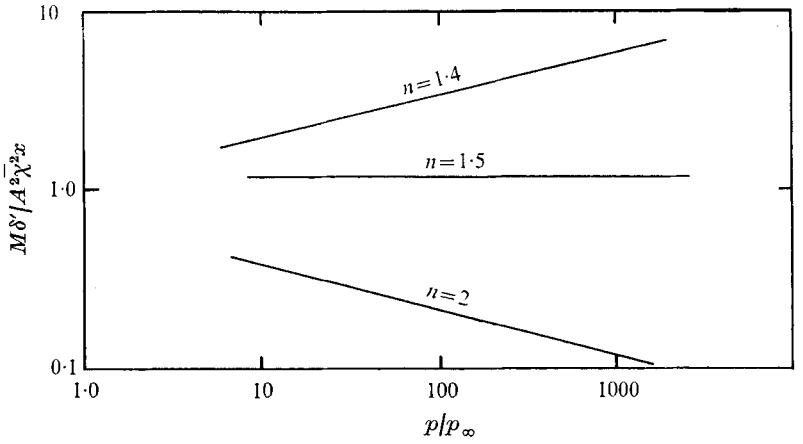

FIGURE 8. Variation of displacement thickness with respect to p/p_∞ over concave surfaces ($y_w \sim x^n$) using the modified Cheng method with $M\alpha = 0{\cdot}3$.

supercritical when $d\delta^*/dp < 0$ and subcritical when $d\delta^*/dp > 0$.) Figure 6 shows the growth of the boundary layer for concave surfaces of the form $y \sim x^n$, obtained using Cheng's method. This figure clearly indicates the super- and subcritical behaviour of the boundary-layer growth over concave surfaces. For $n = \frac{3}{2}$, the displacement thickness remains constant with increasing distance from the leading edge. For $n < \frac{3}{2}$, the boundary-layer behaviour becomes subcritical, i.e. the displacement thickness increases with increasing distance. For $n > \frac{3}{2}$ the boundary layer has a supercritical behaviour. The sub- and supercritical behaviour of the boundary layer for large arguments is also demonstrated in figures 7 and 8, where the displacement thickness is plotted against the surface pressure.

7. Comparisons between the theoretical results and experimental data

Figure 9 compares pressure measurements at $M = 12{\cdot}25$ over the cubic surface with the results from viscous-interaction theory. Cheng's theory predicts pressure fairly well near the leading edge, where the flow field is dominated by the displacement effect, but further downstream, where incidence is the dominant effect, the comparison with Cheng's theory in its original form is not realistic because of the oscillation occurring in the solution. Figure 9 also compares the experimental data with the modified Cheng method. As expected there is no oscillation in the results, the boundary-layer thickness decreasing steadily as the pressure rises. The fairly good agreement between measurement of pressure and the prediction of viscous-interaction theory using the tangent-wedge approximation suggests that the choice of pressure law is important in dealing with the joint effect of viscous interaction and incidence.

Heat-transfer measurements on the cubic model are compared with the predictions of the original and modified Cheng method in figure 10. This figure shows that Cheng's theory compares favourably with our measured heat-transfer rate near

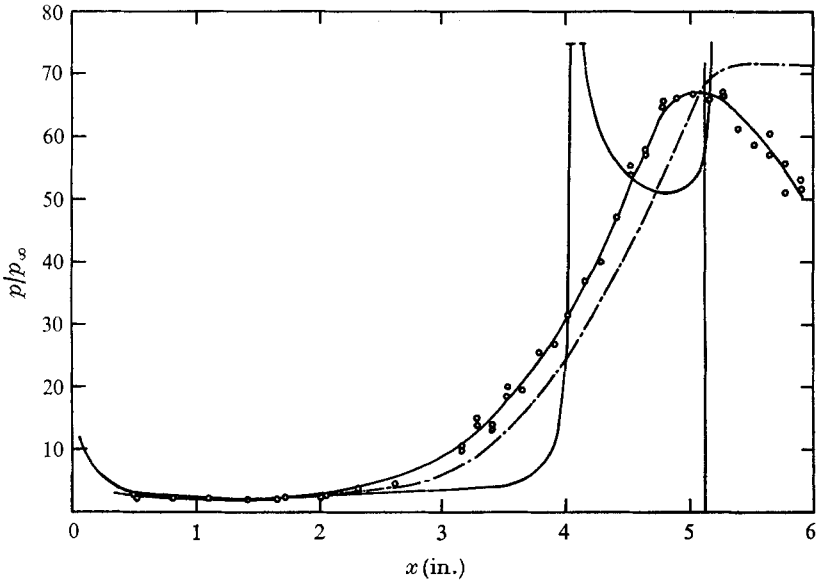

FIGURE 9. Pressure measurements for the cubic surface compared with the results of the viscous-interaction theories; $M = 12{\cdot}25$, $p_0 = 1600$ psia, $T_0 = 1300$ °K, $R = 0{\cdot}86 \times 10^5$. —O—, measurements; ——, Cheng's original method; — · —, modified Cheng method.

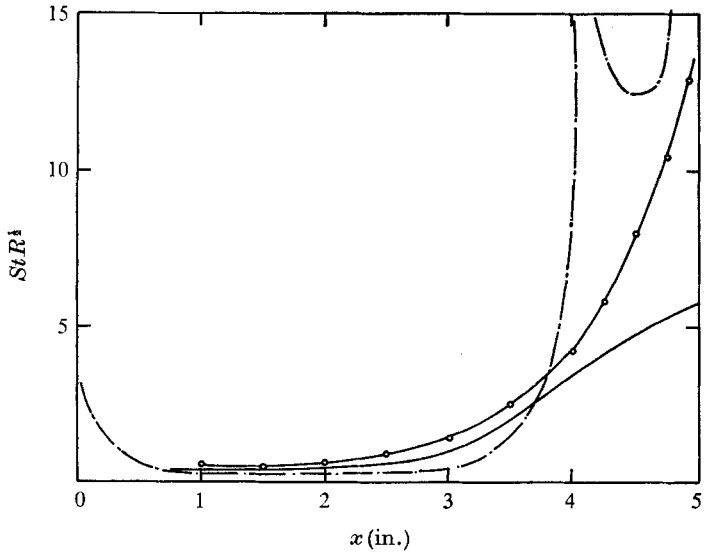

FIGURE 10. Heat transfer on the cubic model; $M = 12{\cdot}25$, $p_0 = 1600$ psia, $T_0 = 1300$ °K, $R = 0{\cdot}86 \times 10^5$. —O—, line through experimental data; — · —, Cheng's original method; ——, modified Cheng method.

the leading edge, but greatly overestimates or underestimates the measurements downstream because of the oscillatory behaviour of the solution. When the more realistic tangent-wedge approximation is used, the heat-transfer prediction shows the right trend but the rate is not adequately predicted in the region of strong adverse pressure gradient, where the boundary-layer profiles are markedly

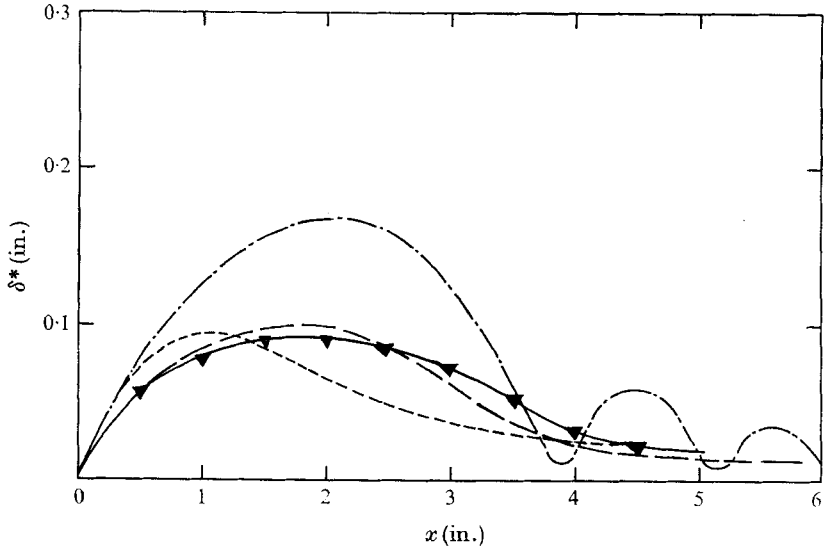

FIGURE 11. Displacement thickness on the cubic model; $M = 12{\cdot}25$, $p_0 = 1600$ psia, $T_0 = 1300\,°\mathrm{K}$, $R = 0{\cdot}86 \times 10^5$, $\alpha = 0$. —·—, Cheng's original method; ——, modified Cheng method; – – –, Sells' (1966) program; —▼—, edge of the boundary layer (taken from photograph).

non-similar. It is not too surprising that Lees' assumption of local flat-plate similarity fails for cases with strong adverse pressure gradients. It may be noted that Lees' solution also assumes that there is no normal pressure gradient. Kepler & O'Brien (1962) and McLafferty & Barber (1959) have measured the static pressure in turbulent boundary layers on concave walls, and Myring & Young (1968) have compared the isobars in those two experiments to the external Mach lines extrapolated into the boundary layer. Myring & Young have shown that the static pressure is constant along Mach lines, and not along normals to the surface. Therefore, strong normal pressure gradients may exist on surface normals.

The oscillations are shown more clearly in figure 11, where the measured displacement thickness from the schlieren photograph is compared with values from the viscous-interaction theories.

For tests of a convex surface the model shown in figure 1(*b*) was used. The wedge angle at the leading edge was 18°, so that the Mach number behind the leading-edge shock was theoretically 4·8. The boundary layer remained attached and laminar, according to the schlieren photographs and heat-transfer records, and grew rapidly but smoothly in the favourable pressure gradient. Figure 12 shows a comparison between measured pressures and those from various theories. Because $M_\infty^2 \alpha^2 / \bar{\chi}_\epsilon \gg 1$ over most of the wedge, the pressure on the wedge is sensibly constant to within 0·3 in. of the leading edge, the nearest point at which measurements were taken. This suggests that strong viscous interaction is confined to a region very close to the leading edge and that elsewhere the flow field is strongly affected by the incidence. This is probably the reason for the good agreement between the tangent-wedge approximation (no viscous interaction)

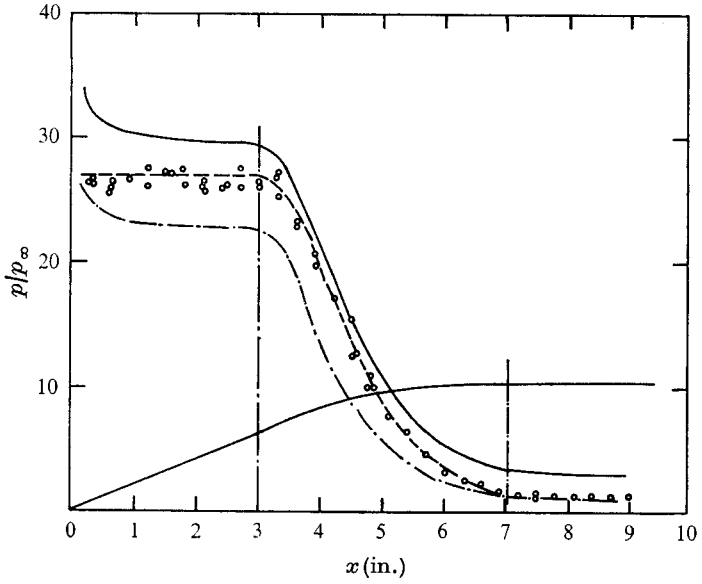

FIGURE 12. A comparison of pressure measurements on the convex model with results from different theories; $M = 12{\cdot}25$, $p_0 = 1600$ psia, $T_0 = 1300$ °K, $R = 0{\cdot}86 \times 10^5$. ○, experimental data; —·—, Cheng's original method, ——, modified Cheng method; – – –, tangent-wedge (inviscid) method.

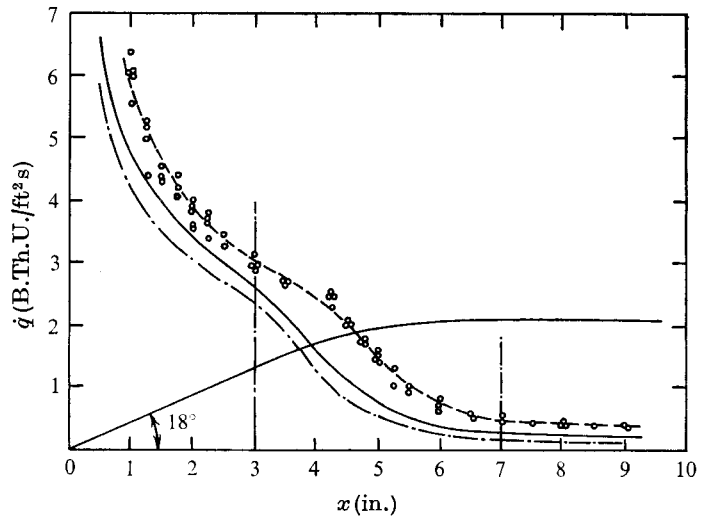

FIGURE 13. A comparison of heat-transfer measurements on the convex model with results from the viscous-interaction theories; $M = 12{\cdot}25$, $T_0 = 1300$ °K, $p_0 = 1300$ psia, $R = 0{\cdot}86 \times 10^5$. ○, experimental data; —·—, Cheng's original theory; ——, modified Cheng method.

and the measurement. Cheng's method does not give an oscillatory solution for convex surfaces, in contrast to the concave case, and, although the pressure prediction is too low over the wedge, it is in a fairly good agreement at the rear part of the model. The modified Cheng method slightly overestimates the pressure on the flat parts of the model, but agrees very well on the expansion shoulder.

Stollery (1970) found almost the same trends when applying viscous-interaction theories to an expansion corner.

Figure 13 gives a comparison between heat-transfer measurement and results from the two viscous-interaction theories, both of which give predictions which are in reasonable agreement with the experimental data. Therefore it appears that the assumption of local flat-plate similarity is possibly reasonable in cases involving favourable pressure gradients.

8. Conclusion

It has been shown numerically and analytically that the viscous-interaction theory due to Cheng *et al.* (1961) gives oscillating solutions for large arguments, when applied to concave surfaces. Therefore this method cannot be used for pressure and heat-transfer predictions over surfaces with adverse pressure gradients. Nevertheless, near the leading edge, where the dominant effect is the displacement thickness, the pressure and heat-transfer predictions from Cheng's method seem to be adequate. A modified Cheng method, which uses a tangent-wedge approximation, does not give oscillatory solution for concave bodies and predicts the surface-pressure distribution reasonably well over the cubic model. It appears that the choice of pressure law is important in any analysis involving viscous interaction. Agreement between heat-transfer measurements and values predicted by the modified method is somewhat less satisfactory in the region of strong pressure gradients, where the boundary-layer profiles are markedly non-similar. Therefore it may be concluded that Lees' similarity solution for the boundary-layer growth is not suitable for heat-transfer prediction in cases of non-similar boundary-layer profiles. Both Cheng's original method and the modified version may be used to predict surface pressure and heat transfer on convex surfaces, although the predictions by the modified version are slightly better. It is also shown that the viscous-interaction theories described in this paper deviate in some cases from the usual assumption of supercritical behaviour of the boundary layers over concave surfaces.

The author would like to thank Mr J. L. Stollery and Prof. N. C. Freeman for their helpful guidance during the course of this study.

REFERENCES

CHENG, H. K., HALL, J. G., GOLIAN, T. C. & HERTZBERG, A. 1961 Boundary-layer displacement and leading-edge bluntness effects in high-temperature hypersonic flow. *J. Aero. Sci.* **28**, 353.

CHENG, H. K. & KIRSCH, J. W. 1969 On the gasdynamics of an intense explosion with and expanding contact surface. *J. Fluid Mech.* **39**, 289–305.

COX, R. N. & CRABTREE, L. F. 1965 *Elements of Hypersonic Aerodynamics.* The English Universities Press Ltd.

HOLDEN, M. S. 1964 Heat transfer in separated flow. Ph.D. thesis, Imperial College, London.

HUNTER, J. A. 1969 Theory and operation of the equipment used at Imperial College to measure heat-transfer rate in hypersonic flow. *Imperial College, Department of Aeronautics, Internal Memo.* 69–001.

KEPLER, C. E. & O'BRIEN, R. L. 1962 Supersonic turbulent boundary-layer growth over cooled walls in adverse pressure gradient. ASD–TDR–62–87.

LEES, L. 1953 On the boundary-layer equations in hypersonic flow and their approximate solutions, *J. Aero. Sci.* **20**, 143.

LEES, L. 1956 Laminar heat transfer over blunt-nosed bodies at hypersonic flight speeds. *Jet Propulsion*, **26**, 259.

MCLAFFERTY, G. & BARBER, R. E. 1959 Turbulent boundary-layer characteristics in supersonic streams having adverse pressure gradient. *United Aircraft Co. Rep.* R–1285–11.

MOHAMMADIAN, S. 1968 Calibration of Mach 12 contoured nozzle. *Imperial College, Department of Aeronautics, Internal Memo.* 68–002.

MOHAMMADIAN, S. 1970 Hypersonic boundary layers in strong pressure gradients. Ph.D. thesis, Aeronautics Department, Imperial College.

MYRING, D. F. & YOUNG, A. D. 1968 The isobars in boundary layers at supersonic speeds. *Aero. Quart.* **19**, 105.

NEEDHAM, D. A. 1963 Progress report on the Imperial College gun tunnel. *ICST Aero. Dept. Rep.* no. 118.

SELLS, C. C. L. 1966 Two-dimensional laminar compressible boundary-layer programme for a perfect gas. *Aero. Res. Counc. R. & M.* no. 3533.

STEWARTSON, K. 1955 On the motion of a flat plate at high speed in a viscous compressible fluid. Part 2. Steady motion. *J. Aero. Sci.* **22**, 303.

STOLLERY, J. L. 1966 The Imperial College gun tunnel. *J. Roy. Aero. Soc.* **64**, 24.

STOLLERY, J. L. 1970 Hypersonic viscous interaction on curved surfaces. *J. Fluid Mech.* **43**, 497–511.

SULLIVAN, P. A. 1968 On the interaction of a laminar hypersonic boundary layer and a corner expansion wave. *U.T.I.A.S. Tech. Note*, no. 129.

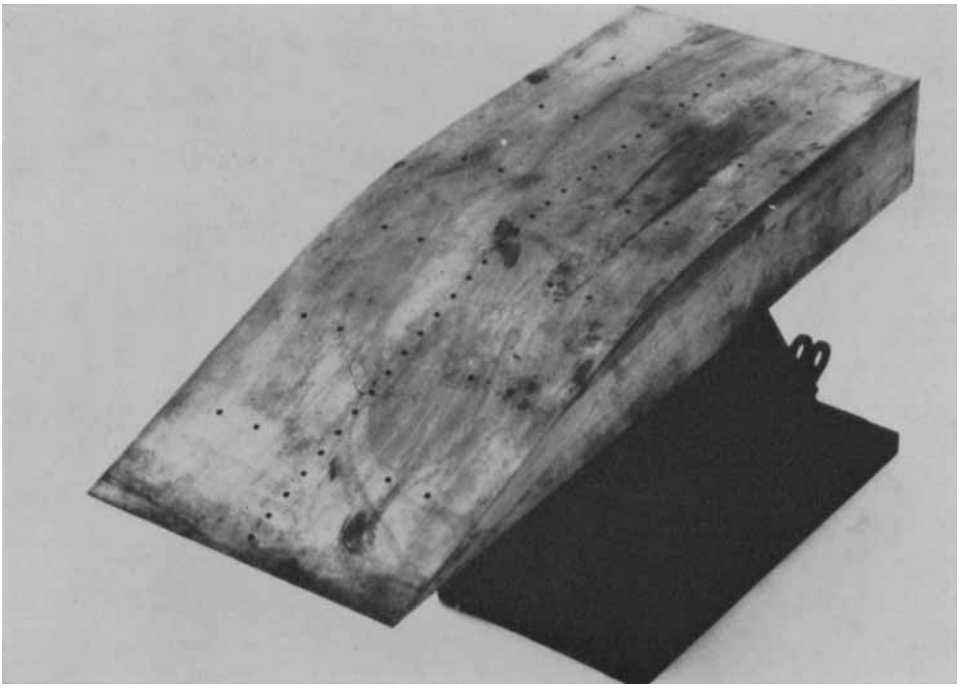

(*a*)

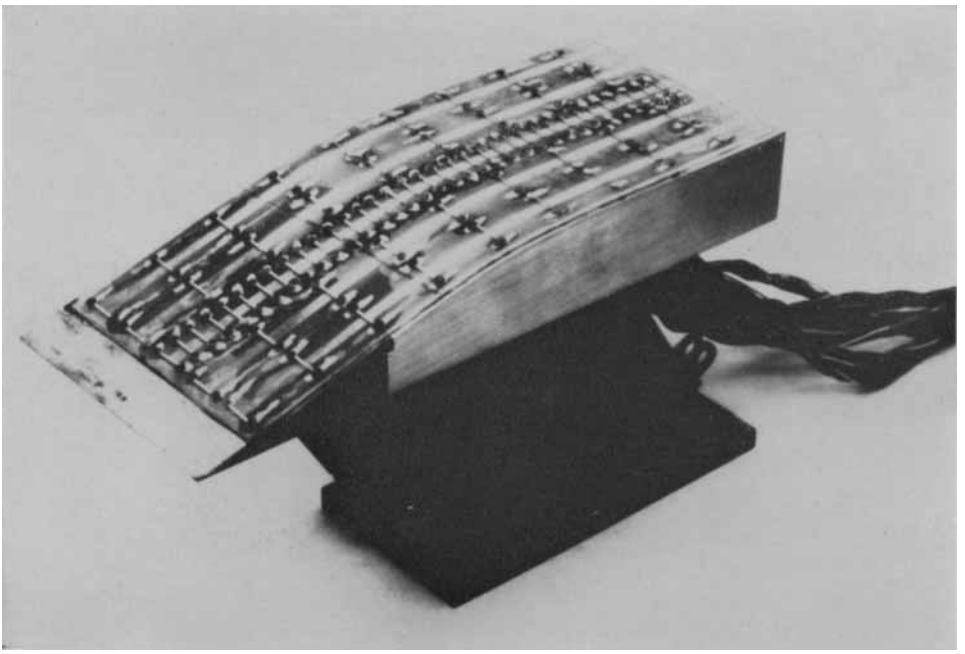

(*b*)

FIGURE 2. Photographs of the convex (*a*) pressure and (*b*) heat-transfer models.

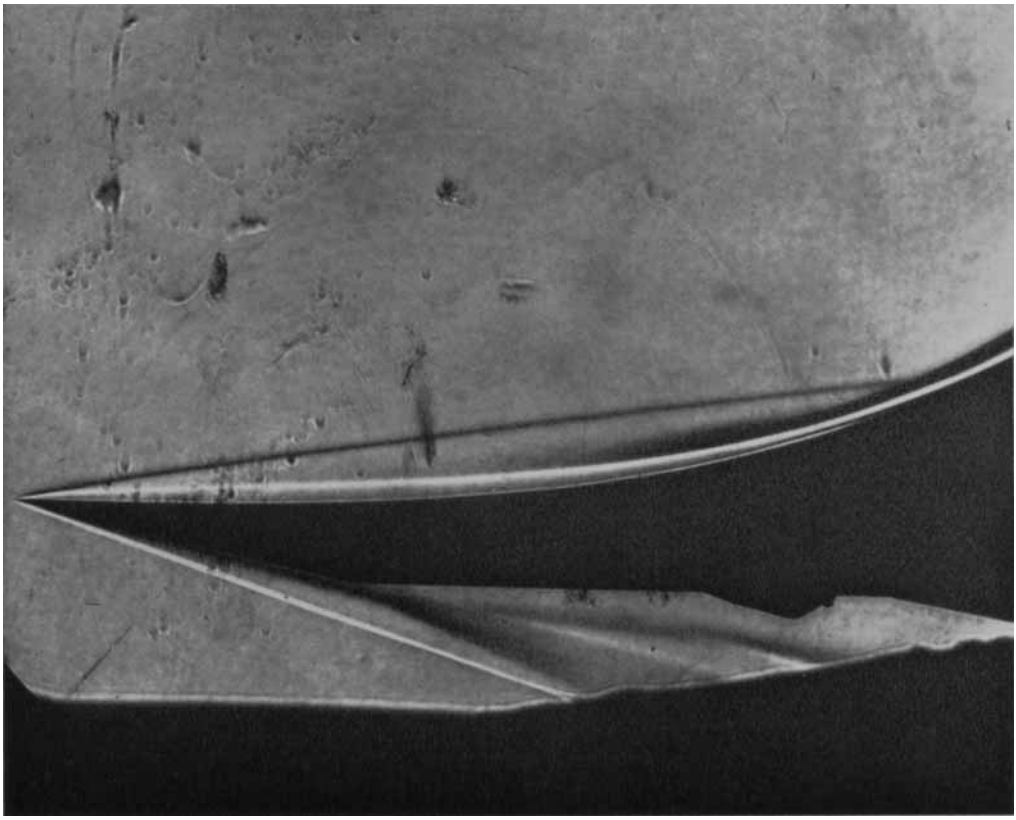

FIGURE 3. Schlieren photograph of flow over the cubic surface; $M = 12{\cdot}25$, $R = 0{\cdot}86 \times 10^5$.

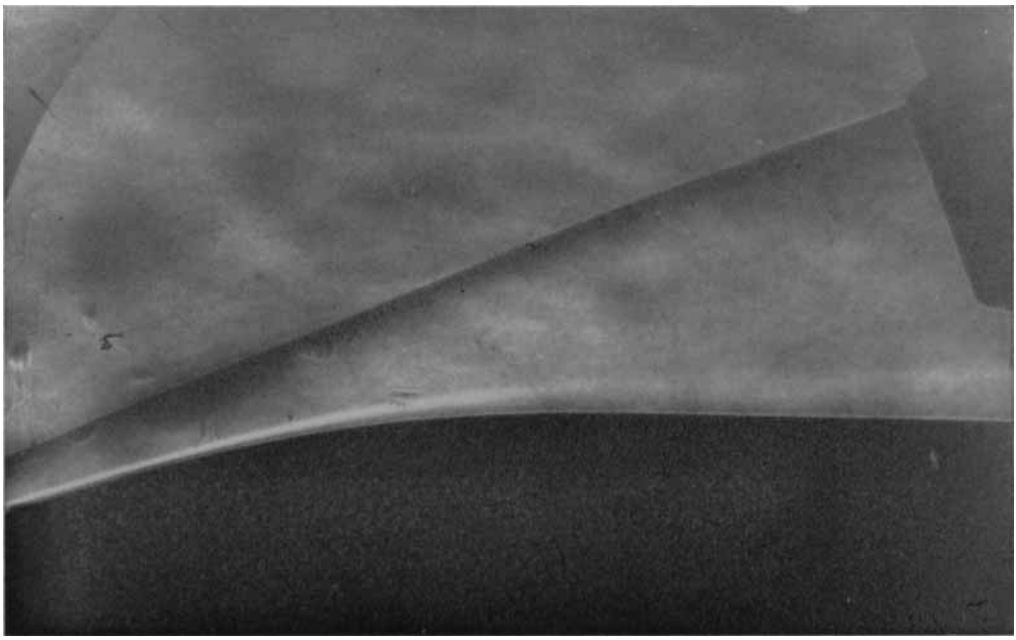

FIGURE 4. Schlieren photograph of flow over the rear part of the convex surface; $M = 12{\cdot}25$, $R = 0{\cdot}86 \times 10^5$.